Supplementary Information

Coupled Model Biases Breed Spurious Low-frequency Variability in the Tropical Pacific Ocean

Dhrubajyoti Samanta[1], Kristopher B. Karnauskas[2,3], Nathalie F. Goodkin[1,4,5], Sloan Coats[6], Jason E. Smerdon[7] and Lei Zhang[3]

1. Asian School of the Environment, Nanyang Technological University, Singapore

2. Cooperative Institute for Research in Environmental Science, University of Colorado Boulder, CO, USA

3. Department of Atmospheric and Oceanic Sciences, University of Colorado Boulder, CO, USA

4. Earth Observatory of Singapore, Singapore

5. Department of Earth and Planetary Sciences, American Museum of National History, NY, USA

6. Department of Geology and Geophysics, Woods Hole Oceanographic Institution, MA, USA

7. Lamont Doherty Earth Observatory, Columbia University, NY, USA

Table caption:

Table S1: Type-1 and Type-2 ENSO models used in this study: Model names; institutes; ocean horizontal mean zonal resolution (at the equator in °E) × mean 25 °N-35 °N resolution in latitude (in °); atmospheric horizontal resolution (in E×N); No. of years; references. Please refer to the Table Appendix 9.A in IPCC WG1 AR5 Chapter 9 for the more information. We chose the same ensemble member from the CMIP5 pi-control runs, where only one run was available for CESM LENS.

Figure caption:

Figure S1: Examples of leading EOF mode (EOF1) of centennial-scale (80-300 years band pass filtered using a Lanczos filter) annual SST from pre-industrial control runs of different models. Models names and variability (in %) are mentioned in the title of each plot. EOFs are expressed in °C per standard deviation. Not all models show a dipole pattern and PCO may exist without a prominent dipole in EOF1 pattern. Therefore, detecting PCO in terms of a dipole pattern in EOF1 of centennial-scale SST may not be appropriate.

Figure S2: Standard deviation of annual unfiltered SST (in °C) for individual models from our study. Legends in each plot indicate the model name.

Figure S3: Same as Figure S2, but for the remaining models from our study.

Figure S4: Scatter plots between equatorial unfiltered DJF SST variability (data same as Figure. 1a, in °C) at the reference longitude 164 °E (REF) with various longitudes. Each dot represents a model. We chose the reference point in the western Pacific because our argument is that the westward extension of ENSO variability (regardless of whether it is due to excessive variability everywhere or not) and related mean-state variability can be related to the emergence of centennial-scale variability over the western Pacific. The selected point in the western Pacific offers a clear separation between two types of models.

Figure S5: Standard deviation of high frequency (10 years high pass filtered using Lanczos filter) annual latent heat flux (in Wm^{-2}) for Type 1, Type 2 ENSO model and their difference (bottom). The first two panels of the figure are an equivalent plot of Figure 3a-b.

Figure S6: Composite standard deviation of low frequency (90-years low pass filtered using Lanczos filter) annual SST (in ºC) for (a) Type-1 and (b) Type-2 ENSO models from historical simulations (1861-2005). All model data are transformed to a common grid of 2.0º ×1.5º before calculating the composite.

Figure S7: Observational equivalent of Figure 3. Standard deviation of (a) high-frequency (10-years high pass filtered using Lanczos filter) annual u10 (in m/s), and (b) low-frequency (90-years low pass filtered using Lanczos filter) annual SST (in °C). The u10 and SST are used from NOAA 20th century v2 data from 1871-2012 and Cobe SST v2 data for 1850-2015, respectively. Despite high zonal wind variability over the western Pacific, there is no centennial-scale variability over the western Pacific. However, a caveat for interpreting centennial variability in observational SST is the insufficient length of the data.

Type-1 Model	Institute	Ocean	Atmosphere	Years	Reference
CESM LENS	NCAR, USA	1.0 × 1.0	1.0 × 1.0	1801	Kay et al. (2015)
BNU-ESM	BNU, China	1.0 × 1.0	2.8 × 2.8	559	Xin et al. (2012)
CanESM2	CCCMA, Canada	1.4 × 0.9	2.8 × 2.8	996	Arora et al. (2011)
CCSM4	NCAR, USA	1.1 × 0.6	1.2 × 0.9	501	Gent et al. (2011)
CSIRO-MK3-6-0	CSIRO-QCCCE, Australia	1.9 × 0.9	1.9 × 1.9	500	Rotstayn et al. (2012)
GFDL-CM3	NOAA-GFDL, USA	1.0 × 1.0	2.5 × 2.0	500	Donner et al. (2011)
GFDL-ESM-2M	NOAA-GFDL, USA	1.0 × 1.0	2.5 × 2.0	500	Donner et al. (2011)
MPI-ESM-LR	MPI-N, Germany	1.5 × 1.5	1.9 × 1.9	1000	Roddatz et al. (2007)
MPI-ESM-P	MPI-N, Germany	1.5 × 1.5	1.9 × 1.9	1156	Roddatz et al. (2007)
Type-2 Model	**Institute**	**Ocean**	**Atmosphere**	**Years**	**Reference**
ACCESS1-3	CSIRO, Australia	1.0 × 1.0	1.9 × 1.2	500	Bi et. al. (2013)
BCC-CSM-1-1	BCC, CMA, China	1.0 × 1.0	2.8 × 2.8	500	Xin et al. (2012)
CESM1-BGC	NCAR, USA	1.1 × 0.6	1.2 × 0.9	500	Long et al. (2012)
CMCC-CMS	CMCC, Italy	2.0 × 2.0	1.9 × 1.9	500	Scoccimarro et al. (2011)
CNRM-CM5	CNRM-CERFACS, France	1.0 × 0.8	1.4 × 1.4	850	Voldoire et al. (2013)
FGOALS-G2	LASG-CESS, China	1.0 × 1.0	2.8 × 2.8	700	Yongqiang et al. (2004)
FGOALS-S2	LASG-IAP, China	1.0 × 1.0	2.8 × 1.7	501	Yongqiang et al. (2004)
FIO-ESM	FIO, SOA, China	1.0 × 0.6	2.8 × 2.8	800	Yongqiang et al. (2004)
GFDL-ESM-2G	NOAA-GFDL, USA	1.0 × 1.0	2.5 × 2.0	500	Donner et al. (2011)
GISS-E2-H	NASA/GISS, USA	1.0 × 1.0	2.5 × 2.0	531	Schmidt et al. (2006)
GISS-E2-R	NASA/GISS, USA	1.2 × 1.0	2.5 × 2.0	550	Schmidt et al. (2006)
HADGEM2-AO	NIMR-KMA, Korea	1.0 × 1.5	1.9 × 1.2	700	Matin et al. (2011)
IPSL-CM5A-LR	IPSL, France	2.0 × 1.9	3.7 × 1.9	1000	Dufresne et al. (2013)
INMCM4	INM, Russia	0.8 × 0.4	2.0 × 1.5	500	Volodin et al. (2010)
MIROC-ESM	AORI-NIES-JAMSTEC, Japan	1.4 × 0.9	2.8 × 2.8	531	Watanabe et al. (2011)
MPI-ESM-MR	MPI-N, Germany	0.4 × 0.4	1.9 × 1.9	1000	Raddatz et al. (2007)
MRI-CGCM3	MRI, Japan	1.0 × 0.5	1.1 × 1.1	500	Yukumoto et al. (2012)
NorESM1-M	NCC, Norway	1.1 × 0.6	2.5 × 1.9	500	Bentsen et al. (2013)

Table S1: Type-1 and Type-2 ENSO models used in this study: Model names; institutes; ocean horizontal mean zonal resolution (at the equator in °E) × mean 25 °N-35 °N resolution in latitude (in °); atmospheric horizontal resolution (in E×N); No. of years; references. Please refer to the Table Appendix 9.A in IPCC WG1 AR5 Chapter 9 for the more information. We chose the same ensemble member from the CMIP5 pi-control runs, where only one run was available for CESM LENS.

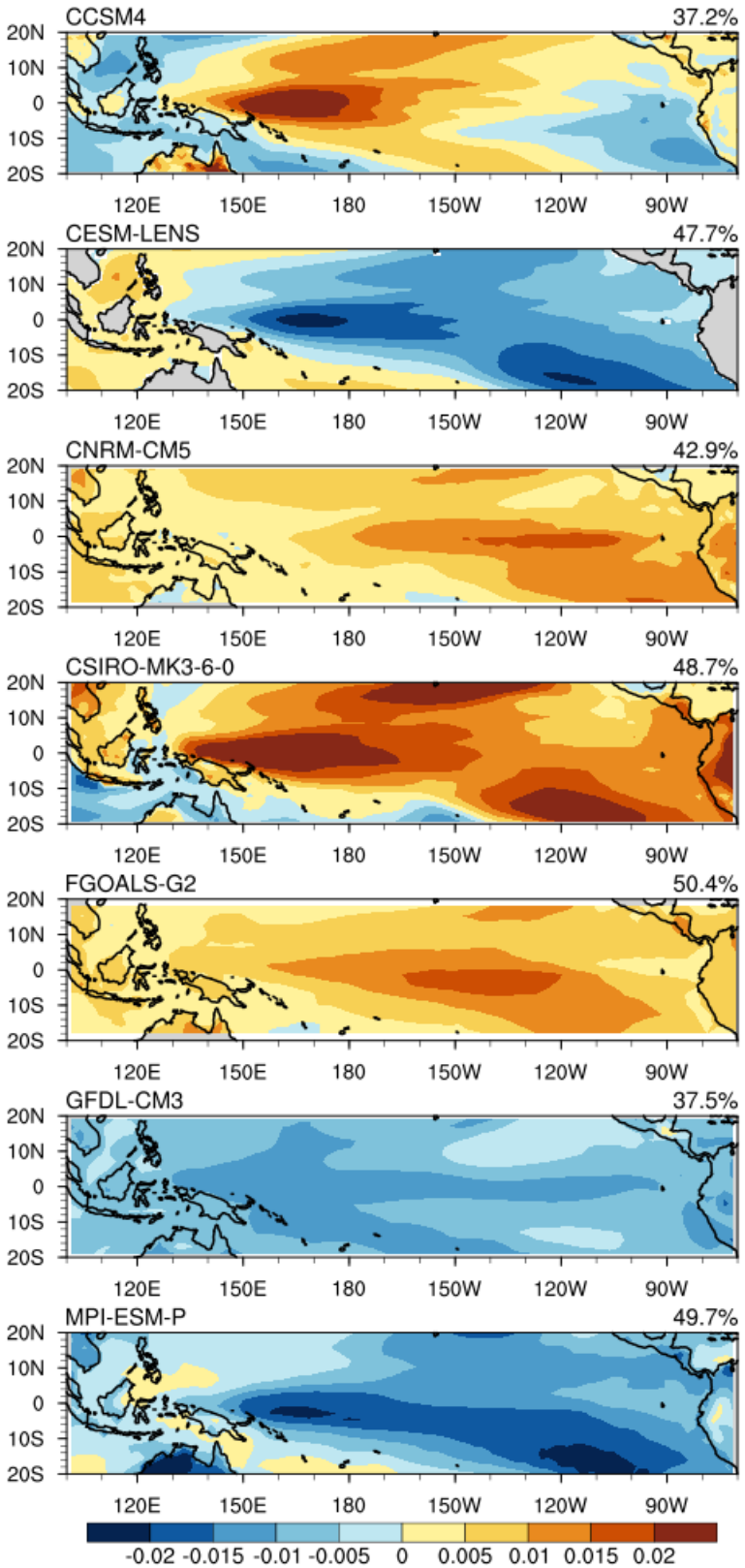

Figure S1: Examples of leading EOF mode (EOF1) of centennial-scale (80-300 years band pass filtered using a Lanczos filter) annual SST from pre-industrial control runs of different models. Models names and variability (in %) are mentioned in the title of each plot. EOFs are expressed in °C per standard deviation. Not all models show a dipole pattern and PCO may exist without a prominent dipole in EOF1 pattern. Therefore, detecting PCO in terms of a dipole pattern in EOF1 of centennial-scale SST may not be appropriate.

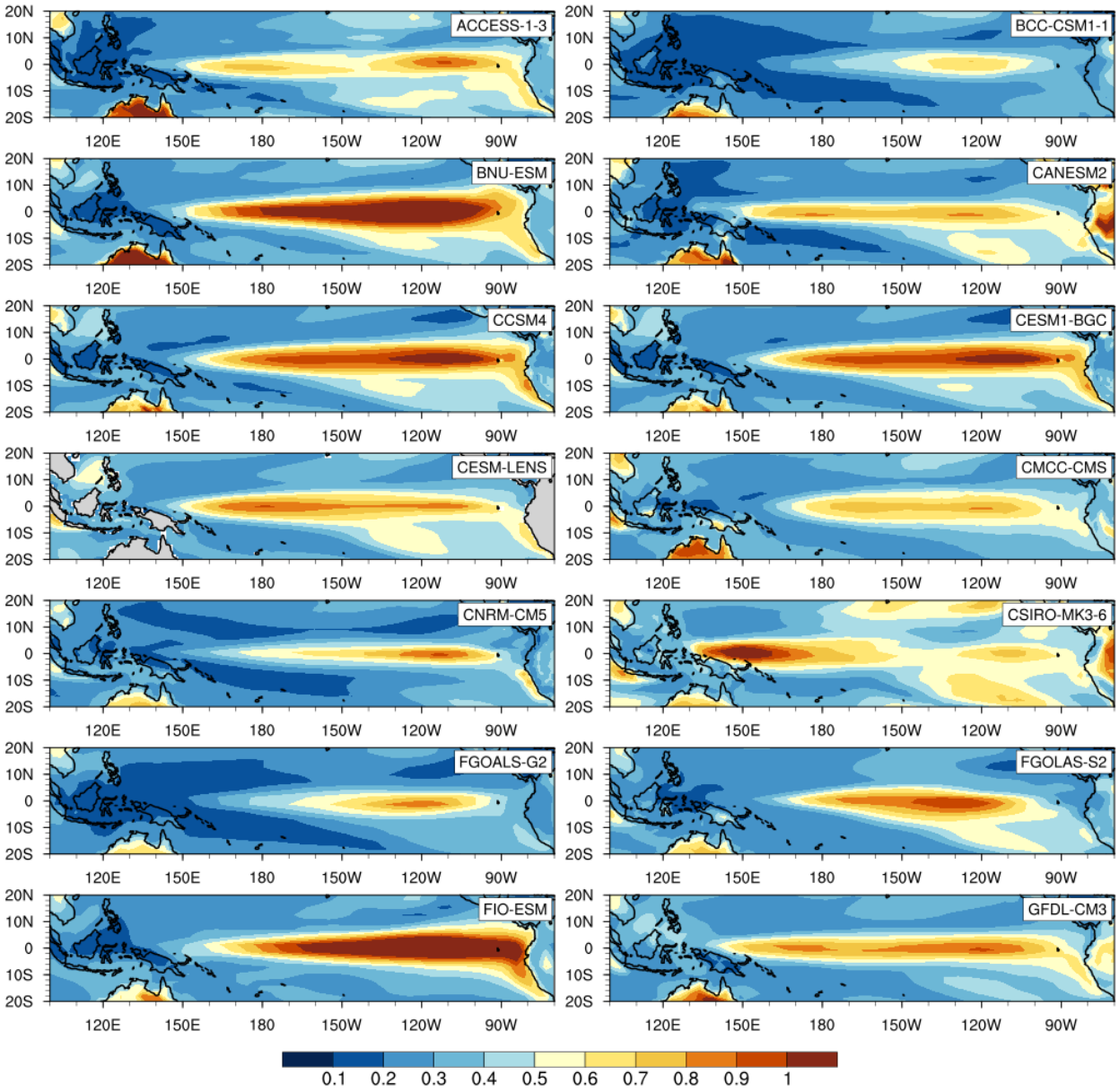

Figure S2: Standard deviation of annual unfiltered SST (in °C) for individual models from our study. Legends in each plot indicate the model name.

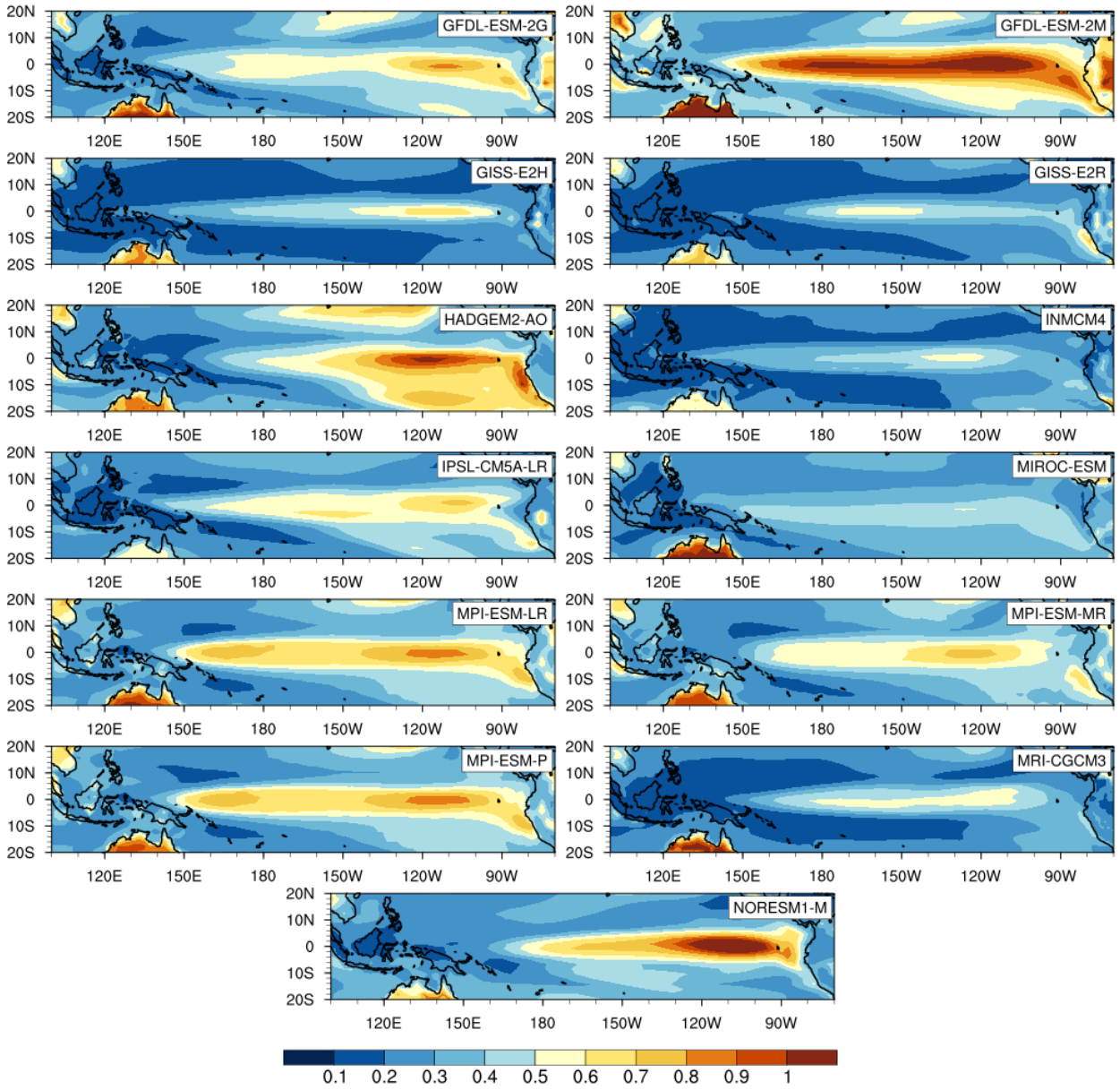

Figure S3: Same as Figure S2, but for the remaining models from our study.

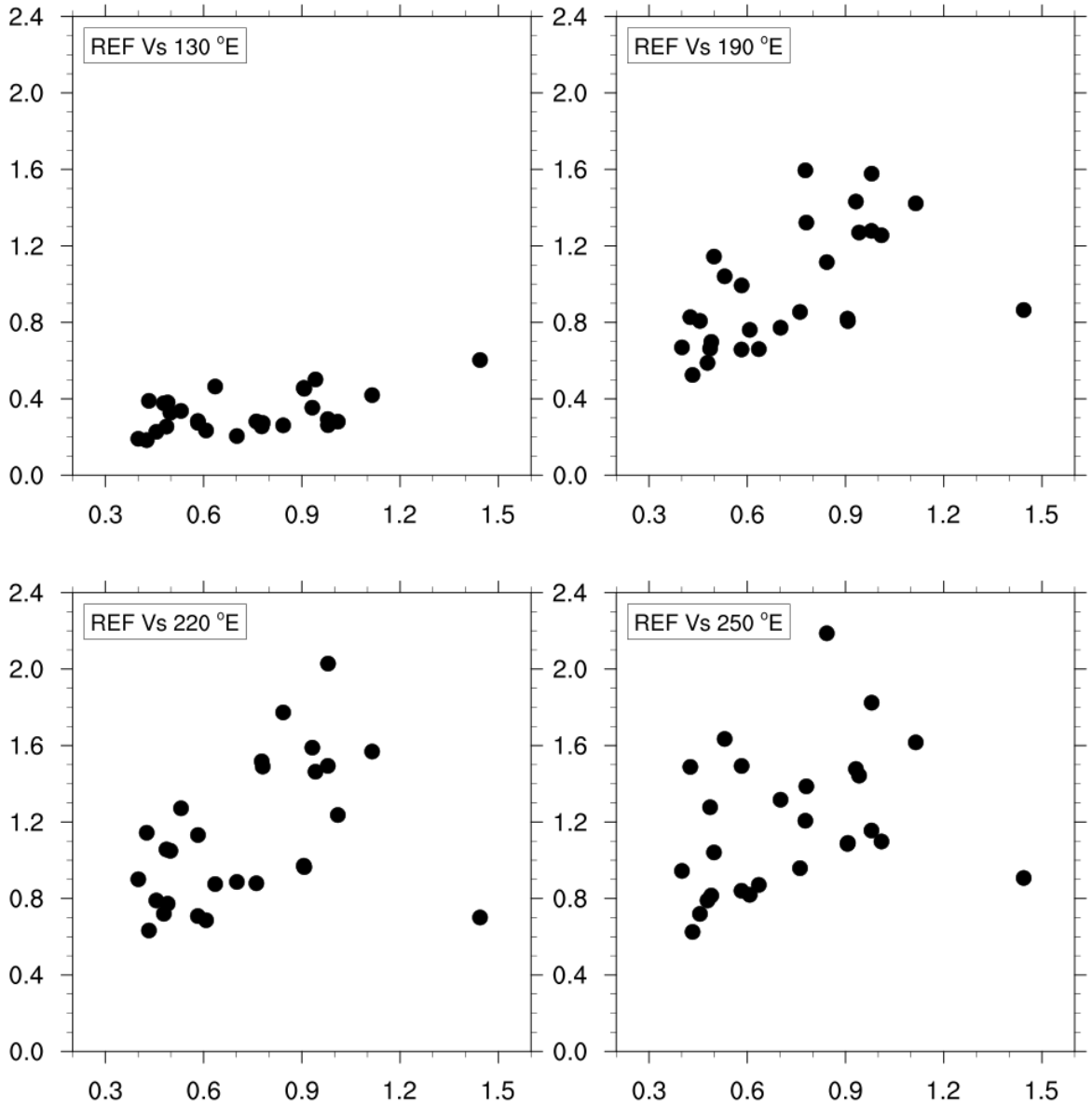

Figure S4: Scatter plots between equatorial unfiltered DJF SST variability (data same as Figure. 1a, in °C) at the reference longitude 164 °E (REF) with various longitudes. Each dot represents a model. We chose the reference point in the western Pacific because our argument is that the westward extension of ENSO variability (regardless of whether it is due to excessive variability everywhere or not) and related mean-state variability can be related to the emergence of centennial-scale variability over the western Pacific. The selected point in the western Pacific offers a clear separation between two types of models.

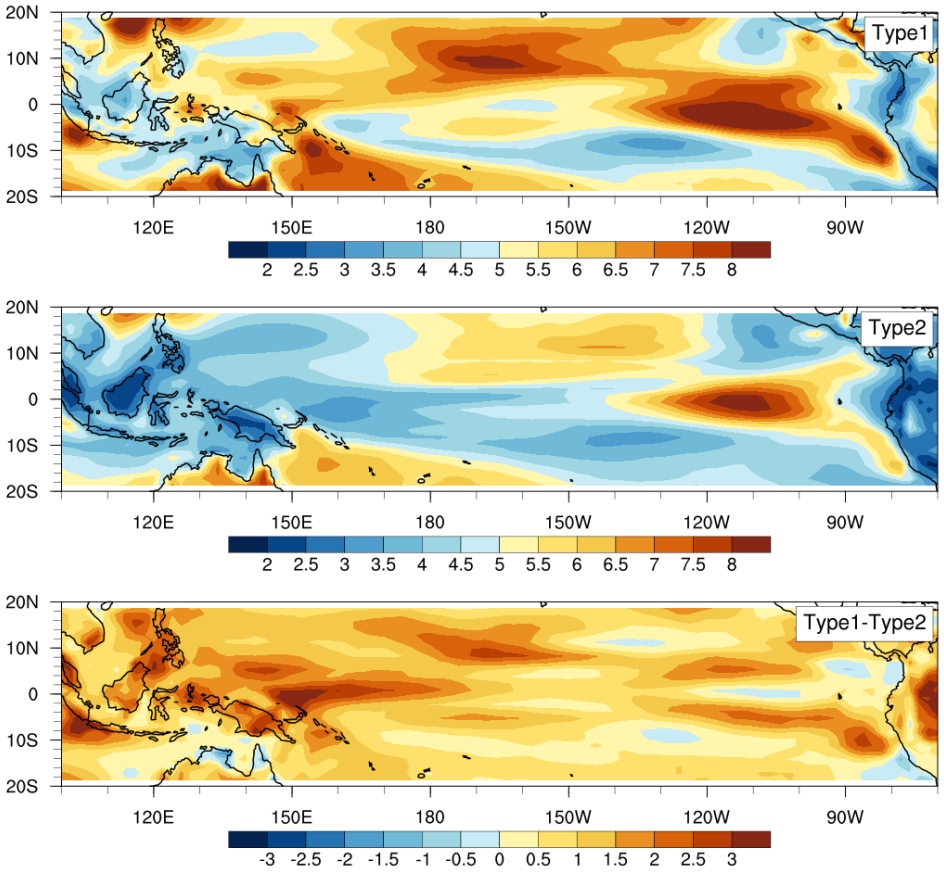

Figure S5: Standard deviation of high frequency (10 years high pass filtered using Lanczos filter) annual latent heat flux (in Wm^{-2}) for Type 1, Type 2 ENSO model and their difference (bottom). The first two panels of the figure are an equivalent plot of Figure 3a-b.

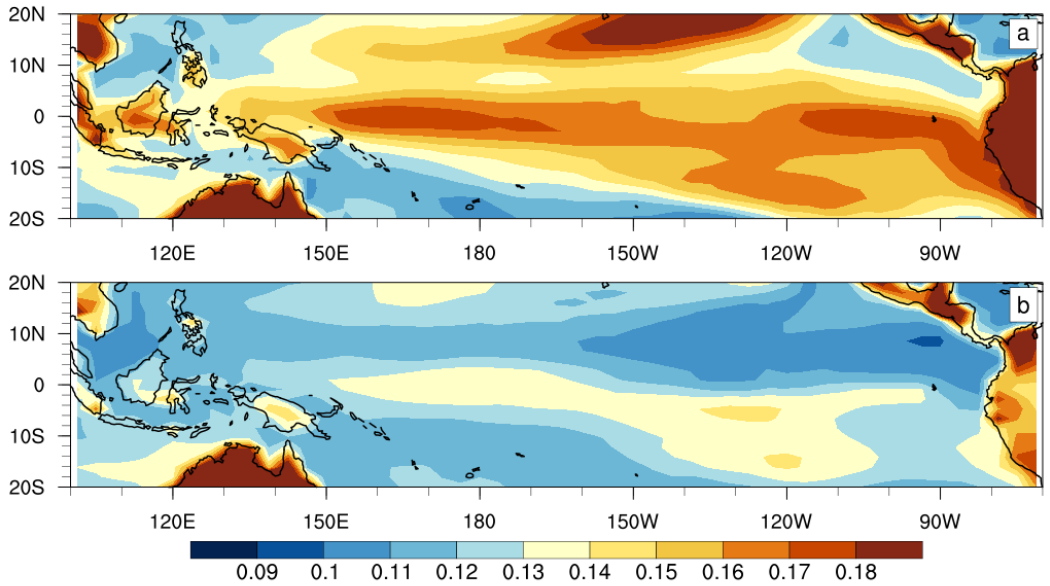

Figure S6: Composite standard deviation of low frequency (90-years low pass filtered using Lanczos filter) annual SST (in ºC) for (a) Type-1 and (b) Type-2 ENSO models from historical simulations (1861-2005). All model data are transformed to a common grid of 2.0º ×1.5º before calculating the composite.

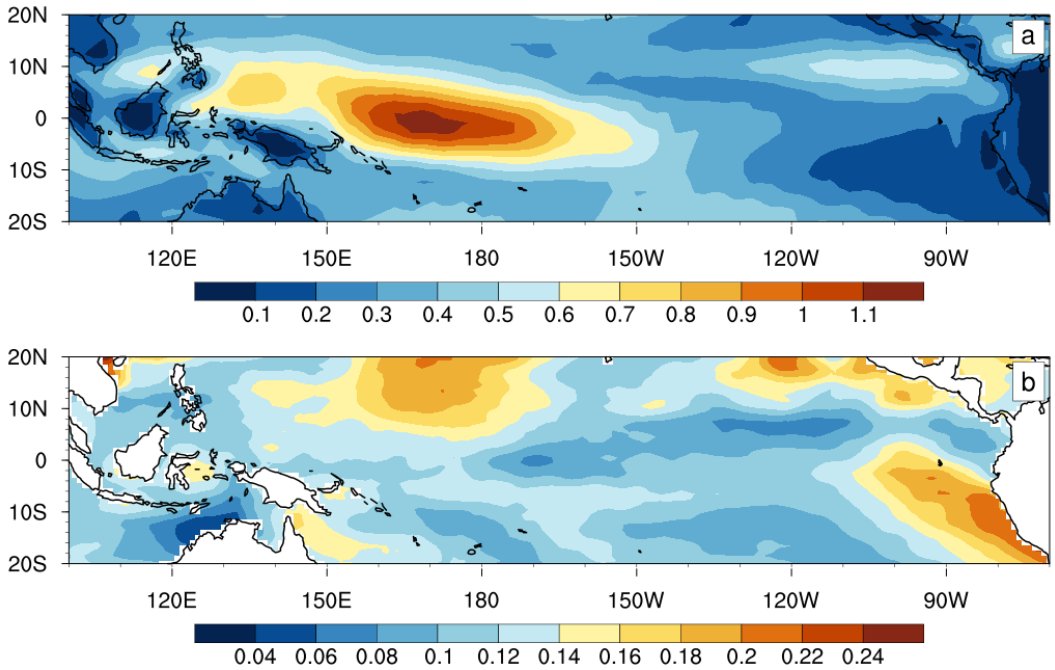

Figure S7: Observational equivalent of Figure 3. Standard deviation of (a) high-frequency (10-years high pass filtered using Lanczos filter) annual u10 (in m/s), and (b) low-frequency (90-years low pass filtered using Lanczos filter) annual SST (in °C). The u10 and SST are used from NOAA 20th century v2 data from 1871-2012 and Cobe SST v2 data for 1850-2015, respectively. Despite high zonal wind variability over the western Pacific, there is no centennial-scale variability over the western Pacific. However, a caveat for interpreting centennial variability in observational SST is the insufficient length of the data.

Derivation of the analytical spectrum of the Hasselmann model

Hasselmann equation can be formulated as follows

$$M\frac{dT(t)}{dt} = LT(t) + F(t) \quad (2)$$

where $M = \rho C_p H$,

ρ is the density of seawater, C_p is the specific heat capacity of seawater, and H is mixed layer depth.

Here the units of M is J/(m^{2}K), $\frac{dT(t)}{dt}$ is K/s, L is J/(m^{2}sK), T(t) is K and F(t) is J/(m^{2}s).

This can be rewritten, $\frac{dT(t)}{dt} = \frac{-L}{M}T(t) + \frac{F(t)}{M}$

And multiplying by $e^{-i2\pi ft}$ and taking integral from $\int_{-\infty}^{+\infty} dt$ gives

$\frac{dT(f)}{dt} = \frac{-L}{M}T(f) + \frac{F(f)}{M}$ where T(f) = $\int_{-\infty}^{+\infty} e^{-i2\pi ft}T(t)dt$ and F(f) has an analogous form.

Taking the derivative on the left-hand side of the equation gives

$-i2\pi fT(f) = \frac{-L}{M}T(f) + \frac{F(f)}{M}$

Or, $T(f)\left(-i2\pi f + \frac{L}{M}\right) = \frac{F(t)}{M}$

Or, $T(t) = \frac{F(t)}{(-i2\pi fM + \lambda)}$

Now, using that power spectral density is $PSD(f) = < T^*(f)T(f) >$, the analytical power spectral density of the Hasselmann model is

$$PSD(f) = \frac{<F^*(f)F(f)>}{(i2\pi fM+\lambda)(-i2\pi fM+\lambda)} = \frac{<F^*(f)F(f)>}{(2\pi fM)^2+\lambda^2} \quad (3)$$

where $< F^*(f)F(f) >$ is the power spectral density of the input noise forcing.

Derivation of the analytical spectrum of the white noise forcing that is the input noise forcing to the Hasselmann model

Using the definition of the Autocorrelation function (ACF) of F(t)

$$ACF(F(t)) = \int_{-\infty}^{+\infty} F(t).F(t+\tau)d\tau; \text{ where } \tau \text{ is the lag} \quad (4)$$

And because F(t) is stationary Gaussian white noise

$$ACF(F(t)) = \sigma^2\delta(\tau) \quad (5)$$

Now, for continuous time, using the Wienner-Khinchin theorem, with the autocorrelation function defined in terms of statistical expected value (as F(t) is stationary). As the process is real valued, the power spectral density of F(t) is

$$\int_{-\infty}^{+\infty} ACF(F(t))e^{-i2\pi f\tau}\, d\tau \quad (6)$$

Now, from (5) and (6), the power spectral density of F(t) is then

147 $$PSD(f) = \sigma^2 \int_{-\infty}^{+\infty} \delta(\tau) e^{-i2\pi f\tau} d\tau = \sigma^2 \quad (7)$$

148 Combining equations (3) and (7), the analytical spectrum of the Hasselmann model is thus, where
149 σ^2 is the variance of the input noise forcing

150 $$PSD(f) = \frac{\sigma^2}{(2\pi f M)^2 + \lambda^2}$$